Optical Stark effect in type-II semiconductor heterostructures

F. Schäfer,[1] A. Trautmann,[2] C. Ngo,[2] J. T. Steiner,[2] C. Fuchs,[3] K. Volz,[3] F. Dobener,[1] M. Stein,[1] T. Meier,[2] and S. Chatterjee[1,*]

[1]*Institute of Experimental Physics I and Center for Materials Research (LaMa), Justus-Liebig-University Giessen, Heinrich-Buff-Ring 16, D-35392 Giessen, Germany*

[2]*Department of Physics, Paderborn University, Warburger Strasse 100, D-33098 Paderborn, Germany*

[3]*Structure & Technology Research Laboratory (WZMW), Philipps-University Marburg, Hans-Meerwein-Straße 6, D-35032 Marburg, Germany*

(Received 9 October 2023; accepted 16 January 2024; published 2 February 2024)

Charge-transfer excitons feature a permanent dipole moment introduced by the spatial charge separation of electron and hole wave functions. This directly influences and qualitatively modifies the coherent nonlinear optical response monitored in high-quality (Ga, In)As/Ga(As, Sb) type-II heterostructures through an optical-pump optical-probe experiment. A microscopic analysis based on the semiconductor Bloch equations reveals that the spatial inhomogeneity native to such type-II heterostructures introduces already on the Hartree-Fock a finite coupling between excitons of opposite spins which is pivotal for optical Stark effect experiments. This result in a blueshift of the charge-transfer exciton when pumping below the resonance for both, co-circular and counter circular polarization configurations, contrary to well-known and observed shifts of spatially direct exciton resonances.

DOI: 10.1103/PhysRevB.109.075301

I. INTRODUCTION

The nonlinear optical response of excitons has been a topic of great interest in condensed-matter physics for several decades [1,2]. In particular, the nonlinear optical response of spatially direct excitons has been extensively investigated. These quasiparticles dominate the spectral responses in the vicinity of the band gap and are very pronounced in low-dimensional systems such as two-dimensional (2D) materials or, historically, in type-I semiconductor quantum well (QW) systems. The quality of the latter structures have been continuously advanced for many decades, which has consistently led to a deeper understanding of the underlying microscopic physics [1,3–5]. Consequently, semiconductor QW structures are at the heart of many virtually indispensable devices such as semiconductor lasers. This presumably most wide-spread technological application relies on population inversion or, physically speaking on the charge-carrier dynamics. Others, particularly switching applications more often rely on even faster electric field related effects such as the quantum-confined Stark effect [6]. It is widely used in the development of electro-optic modulators [5,7], optical switches [8,9], opto-electronic logic [10], and similar devices. The related optical Stark effect in semiconductor quantum structures is lately being applied in the growing fields of quantum information processing [11,12] and quantum cryptography [13,14].

Recently, high-quality type-II heterostructures featuring spatially indirect charge-transfer excitons (CTXs) as the lowest-energy resonances have become available [15–18]. These structures are composed of two different materials with different band offsets, creating a type-II band alignment at their interface. This inherently results in a spatial separation of the electron wave functions and the hole wave functions. In turn, several significant differences compared with the established type-I QW systems result such as the CTXs featuring a nonzero permanent dipole moment. Most prominently, however, the type-II transition is shifted toward lower energies. Consequently, such heterostructures appear ideal for laser applications in the near infrared and midinfrared, e.g., as active media in W-type semiconductor laser structures [19–21]. They feature a broad gain bandwidth [18] while exhibiting lower Auger losses in the constituent materials [22–24]. These advantageous features should also render such structures viable candidate systems for other devices exploiting their nonlinearities. However, their coherent nonlinear response remains virtually unexplored to date. Previous studies on the influence of carrier-order correlation effects have focused on pump-probe (PP) experiments in type-I heterostructures [25–28]. To comprehend the fundamental physical properties of CTXs more closely, it is essential to consider the spatially separated excitations, which inherently result in a net permanent dipole moment. Furthermore, they exhibit a finite coupling between excitons with opposite spins, which is already present on the Hartree-Fock (HF) level [29]. This coupling plays a crucial role for absorption changes when opposite circularly polarized pump and probe pulses are employed for studying the optical Stark effect.

In this paper, we discuss the influence of carrier-correlation effects on the pump-induced absorption and present an analysis in the coherent $\chi^{(3)}$ limit [26,27,30–36]. Section II presents the type-II QW structure, including the relevant selection

*sangam.chatterjee@physik.uni-giessen.de

rules, gives the relevant details about the PP setup, summarizes the experimental parameters, and presents prototypical data for the nonlinear optical response. These are analyzed using a microscopic theory based on the semiconductor Bloch equations (SBE) [34,35] incorporating coherent biexcitonic many-body correlations up to the third order in the optical fields. Section III, introduces this, briefly describing the one-dimensional (1D) tight-binding model by introducing the relevant equations of motion to determine the nonlinear response within the coherent $\chi^{(3)}$ limit. This work focuses on the nonlinear optical response of CTX resonance for excitations detuned below its transition energy and compares with the established observations for the energetically higher type-I exciton transitions as a reference. Varying the magnitude of the permanent dipole moment contribution clearly dominates the spectral changes observed at the CTX transition energies while having virtually no influence on the spatially direct transitions because they do not feature any such contribution. The comparison of the differential absorption spectra in Sec. IV shows the qualitatively excellent agreement between experiment and theory. The microscopic analysis thus clearly reveals that the spatial inhomogeneity native to CTXs results in additional Coulomb related contributions. Therefore, these additional contributions to the pump-induced absorption changes need to be considered even at the HF level to correctly describe the CTX dynamics for all high-quality systems containing charge-transfer contributions, including molecular heterostructures or 2D heterostructures unless such intricate intrinsic spectral features are fogged by disorder or defect-related signatures.

II. EXPERIMENTAL SETUP AND PROCEDURES

A 5 kHz repetition rate regenerative amplifier system generates 50 fs pulses centered around 800 nm with a pulse energy of 1.6 mJ. Approximately 30% of the amplifier emission is used to generate a white-light supercontinuum in a 6-mm-thick sapphire crystal, while the remaining 70% drives an optical parametric amplifier (OPA). The main output of the OPA provides short pulses with tunable central wavelength. These are spectrally tailored, using a grating pulse shaper set up in reflection geometry, to a full width at half maximum (FWHM) of about 2.71 meV/1.6 nm resulting in a pulse duration of 1.04 ps. The excitation beam is focused onto the sample to a spot size of 300 μm diameter. The sample is held at liquid helium temperatures in a cold-finger cryostat. A wedge beam splitter divides the white-light beam into two. One part serves as a reference pulse which is directly propagated to the spectrometer. The other part is focused to a spot diameter of 200 μm on the sample where it probes the sample's excitation-induced absorption changes. Both white-light beams are spectrally analyzed using an imaging spectrometer equipped with a 600 lines/mm grating and a scientific complementary metal-oxide semiconductor (sCMOS) camera (see Fig. 1). It has 2160 lines that can be read out individually and allows multiple lines to be combined into a region of interest (ROI). The imaging allows for reading out both pulses simultaneously and independently. This enables the comparison of spectra between the two pulses, leading to the calculation of a transfer function T_f that converts the spectrum of the reference

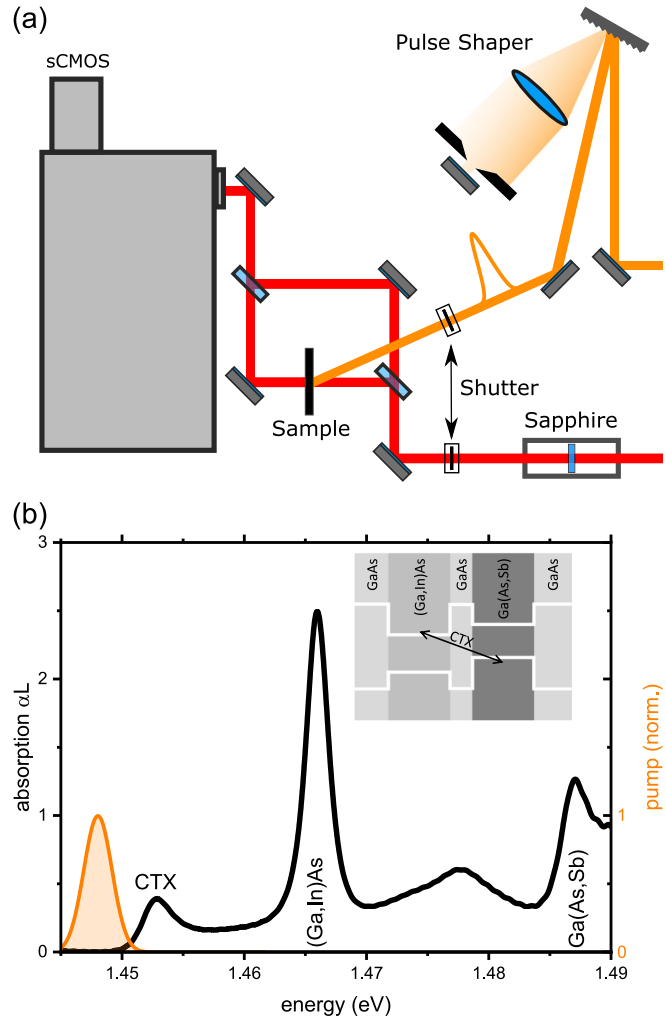

FIG. 1. (a) Schematic of the experimental setup for optical pump-optical probe measurements, incorporating a pulse shaper for the pump pulse. Two wedge beam splitters are employed to establish a reference path, compensating for white-light fluctuations, in conjunction with a sCMOS chip and a transfer function. Mechanical shutters are utilized to capture background and photoluminescence spectra, as well as to measure the transmission through the sample. (b) The linear absorption spectrum of the sample (black line) superimposed with the applied pump pulse (shaded orange) at an energy of 1.448 eV (4.8 meV below the CTX). The inset illustrates the schematic band structure of the sample, emphasizing the spatially indirect CTX transition indicated by an arrow within a type-II heterostructure system.

pulse (T_{ref}) into the spectrum of the pulse transmitted through the unexcited sample. Consequently, introducing the optical excitation then simultaneously determines the transmission through the excited sample (T_{P}) and the transmission through the unexcited sample (T_0). Taking into account the photoluminescence background (T_{Pl}) and the scattered light background (T_{Bg}) in both paths at the beginning of each set of pump pulse parameters then yields the differential absorption $\Delta\alpha L$ for each time step according to

$$\Delta\alpha L = -\ln\left(\frac{T_{\mathrm{P}} - T_{\mathrm{Pl}}}{T_{\mathrm{f}}\left(T_{\mathrm{ref}} - T_{\mathrm{Bg}}\right)}\right). \tag{1}$$

Furthermore, removing the sample from the beam path yields the transfer function that converts the reference path to the spectrum of the pulse transmitted through the sample holder. The sample is then placed back into the beam path, allowing us to measure the transmission through the unexcited sample and calculate the linear absorption.

The sample under investigation is a type-II band alignment multi QW sample grown using metal organic vapor phase epitaxy in an AIXTRON AIX 200 Gas Foil Rotation (GFR) reactor system. The active layer of the type-II system comprises 50 repetitions of compressively strained (Ga, In)As/GaAs/Ga(As, Sb) layers, which are separated by thick, tensilely strained GaAs/Ga(As, P)/GaAs barriers. The latter provide strain compensation and electronic decoupling of the individual repetitions. High-resolution x-ray diffraction and atomic force microscopy analyses confirm the layer thicknesses of 7.7, 7.5, and 1 nm for $Ga_{0.942}In_{0.058}As$, $GaAs_{0.967}Sb_{0.033}$, and the GaAs interlayer, respectively [15]. In these compositions, the maximum of the electron wave function in the conduction band is in the (Ga, In)As layer, while the center-of-gravity of the highest energy hole wave function in the valence band is in the Ga(As, Sb) layer. The intentionally low concentrations of In and Sb result in shallow QWs with depths of only a few tens of meV. In combination with the electronically almost negligible thin interlayer, this leads to a significant overlap of the electron and hole wave functions. Consequently, these high-quality heterostructures show several clearly resolved resonances in the linear absorption spectrum, exhibiting significant oscillator strength. The lowest-energy transition is associated with the CTX and is clearly visible despite the lower oscillator strength expected for spatially separated transitions. The higher-energy resonances are associated with spatially direct exciton transitions. Figure 1 shows the linear absorption of the unexcited type-II sample (black line). The linear absorption spectrum reveals three distinct peaks at 1.452, 1.467, and 1.487 eV. The lowest energy peak corresponds to the CTX transition, the other two to the type-I heavy-hole exciton peak in the (Ga, In)As layer and the Ga(As, Sb) layer, respectively. A fourth peak at 1.478 eV is attributed to the transition from the first hole state in Ga(As, Sb) to the second electron state in the (Ga, In)As quantum well. The light holes are intentionally shifted to higher energies due to residual strain to result in more clear polarization-resolved features.

III. THEORETICAL DESCRIPTION

The SBE represent a powerful framework to describe the optical properties of virtually all semiconducting systems. Due to their microscopic nature, i.e., the inclusion of relevant states and processes in the system Hamiltonian and the systematic treatment of many-body interactions, they even offer predictive capabilities including the interplay and formation as well as decay dynamics of many-body correlations [37,38].

The description of heterostructures featuring charge-transfer excitons requires the inclusion of a nonlocal dipole interaction, i.e., the permanent dipole moment of the charge-transfer exciton in addition to its interband transition dipole moment. This permanent dipole moment is not present for quasiparticles in spatially symmetric systems such as excitons in type-I quantum wells.

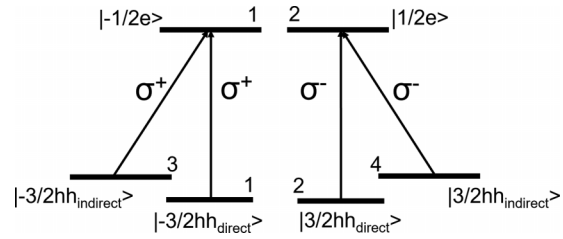

FIG. 2. Schematical illustration of the energetically lowest optical interband transitions within a type-II QW system. The selection corresponds to zincblende materials, such as GaAs-based semiconductor nanostructures. The numbers label the considered heavy-hole valence bands and the conduction bands.

Therefore, to theoretically describe the optical excitations of the type-II quantum-well system investigated here, besides spatially direct optical intrawell transitions, also spatially indirect optical interwell transitions need to be considered. In the latter process, the photoexcitation moves the electron from one well to the other. The interband excitations with the lowest energies can qualitatively be described by the six level scheme given in Fig. 2. This scheme visualizes the relevant polarization selection rules for the interband transitions that start from the energetically highest heavy-hole bands of the two quantum wells. The type-I intrawell optical transitions are given by the well-established selection rules for zincblende materials near the Γ point, i.e., circularly polarized light labeled by the subscripts "direct" [34,35]. The spatially indirect transitions of the type-II heterostructure are accounted for by including two additional valence bands ($v_{3,4}$) which are located in the other well. These optical transitions also follow the well-established selection rules for zincblende materials, i.e., involve circularly polarized transitions which are labeled by the subscripts "indirect." As described in Sec. II, in the investigated type-II heterostructure the transition frequency of the indirect excitations is smaller than that of the direct excitations.

It has been shown in several previous studies that many-body correlations, i.e., terms describing effects of the many-body Coulomb interaction beyond the time-dependent Hartree-Fock approximation, are required in order to properly describe the dependence of pump-probe and four-wave-mixing experiments on the polarization directions of the incident pulses, see, e.g., Refs. [26,27,33,34,35].

In this paper, we include biexcitonic coherences which represent four-particle correlations within the framework of the coherent $\chi^{(3)}$ limit in our theoretical and numerical analysis. Numerically, we evaluate the resulting SBE for a one-dimensional tight-binding model, see, e.g., Refs. [26,27,34–36].

We extend the models used previously by adding the indirect transitions including the permanent dipole moment of the charge-transfer exciton.

The Hamiltonian that describes the nonlinear optical response is given by [34,35]

$$\hat{H} = \hat{H}_0 + \hat{H}_{L-M} + \hat{H}_{\mathrm{C}}. \tag{2}$$

It includes the single-particle Hamiltonian $\hat{H}_0$, the dipole interaction between light and matter $\hat{H}_{L-M}$, and the many-body Coulomb interaction $\hat{H}_C$. The Hamiltonian $\hat{H}_C$ contains the repulsion between electrons, the repulsion between holes, and the electron-hole attraction and gives rise to the formation of bound electron-hole complexes such as excitons and biexcitons.

As is well known, the many-body Coulomb interaction $\hat{H}_C$ introduces an infinite hierarchy problem where lower-order equations of motion couple to higher orders. Here, we truncate the many-body hierarchy by limiting the optical response to the third-order and additionally assume fully coherent dynamics, i.e., we apply the dynamics-controlled truncation scheme to obtain the SBE in the coherent $\chi^{(3)}$ limit [18,26,27,30,32,34–36].

This yields a closed set of differential equations that describe the coupled dynamics of single-exciton p_{12}^{vc} and two-exciton coherences $\overline{B}_{ba12}^{v'c'vc}$. For the one-dimensional tight-binding model the equation of motion for the single-exciton coherence reads [26,35,36]

$$\begin{aligned}
-i\hbar\frac{d}{dt}p_{12}^{vc} = &-\sum_j T_{2j}^{c} p_{1j}^{vc} - \sum_i T_{i1}^{v} p_{i2}^{vc} + V_{12}^{vc} p_{12}^{vc} \\
&+ \mathbf{E}(t)\cdot\Big[\left(\mu_{12}^{vc}\right)^* - \sum_{abv'c'}\left(\mu_{1b}^{vc'}\right)^*\left(p_{ab}^{v'c'}\right)^* p_{a2}^{v'c} \\
&+ \left(\mu_{b2}^{v'c}\right)^*\left(p_{ba}^{v'c'}\right)^* p_{1a}^{vc'}\Big] \\
&+ \sum_{abv'c'}\left(V_{a2}^{c'c} - V_{a1}^{c'v} - V_{b2}^{v'c} + V_{b1}^{v'v}\right) \\
&\times\left[\left(p_{ba}^{v'c'}\right)^* p_{b2}^{v'c} p_{1a}^{vc'} - \left(p_{ba}^{v'c'}\right)^* p_{ba}^{v'c'} p_{12}^{vc}\right. \\
&\left.- \left(p_{ba}^{v'c'}\right)^* \overline{B}_{ba12}^{v'c'vc}\right]. \qquad (3)
\end{aligned}$$

Here, the subscripts i and j denote sites in real space. The considered relevant valence and conduction bands are labeled by $v = 1, 2, 3, 4$ and $c = 1, 2$, respectively, see Fig. 2. The matrices $T_{i,j}^{v/c}$ include the energies of electrons and holes on their diagonals and the tight-binding coupling in the first off-diagonals. The equation of motion for the single-exciton amplitude, Eq. (3), includes in the first line the band energies and tight-binding couplings, and the electron-hole attraction V_{12}^{vc}. The second and third lines of Eq. (3) describe the light-matter interaction including the linear source term $[\mathbf{E}(t)\cdot\boldsymbol{\mu}]$ and nonlinearities which are known as Pauli-blocking or phase-space filling $[\mathbf{E}(t)\cdot\boldsymbol{\mu}p^*p]$ [34,35,39]. The Coulomb interaction gives rise to two inhomogeneities, the first-order Coulomb interaction ($CI_{1st} \propto p^*pp$), which represents a nonlinearity that arises in the time-dependent Hartree-Fock approximation, and the term ($CI_{\mathrm{corr}} \propto Vp^*B$) [26,33], which describes biexcitonic many-body correlations. Due to the additive appearance of the different inhomogeneities in Eq. (3) the contributions to the differential absorption from the three nonlinear processes can be analyzed separately and the total signal is simply given by their sum. The equation of motion for the two-exciton coherence $\overline{B}_{ba12}^{v'c'vc}$ is given by [26,35,36]

$$\begin{aligned}
-i\hbar\frac{d}{dt}\overline{B}_{ba12}^{v'c'vc} = &-\sum_i\Big(T_{2i}^{c'}\overline{B}_{ba1i}^{v'c'vc} + T_{i1}^{v'}\overline{B}_{bai2}^{v'c'vc} \\
&+ T_{ai}^{c'}\overline{B}_{bi12}^{v'c'vc} + T_{ib}^{v'}\overline{B}_{ia12}^{v'c'vc}\Big) \\
&+ \left(V_{ba}^{v'c'} + V_{b2}^{v'c} + V_{1a}^{vc'} + V_{12}^{vc}\right. \\
&\left.- V_{b1}^{v'v} - V_{a2}^{c'c}\right)\overline{B}_{ba12}^{v'c'vc} \\
&- \left(V_{ba}^{v'c'} + V_{12}^{vc} - V_{b1}^{v'v} - V_{a2}^{c'c}\right)p_{1a}^{vc'}p_{b2}^{v'c} \\
&+ \left(V_{1a}^{vc'} + V_{b2}^{v'c} - V_{b1}^{v'v} - V_{a2}^{c'c}\right)p_{ba}^{v'c'}p_{12}^{vc}. \qquad (4)
\end{aligned}$$

The first two lines of Eq. (4) contain the electronic energies and the tight-binding couplings. The third line includes the six terms describing the Coulomb interaction between the four particles, i.e., the four attractive electron-hole interaction terms and the two repulsive ones between two electrons and two holes, respectively. The two-exciton amplitude $\overline{B}_{ba12}^{v'c'vc}$ describes both bound biexcitons, which can form by the attractive interaction between two excitons with opposite spin, and unbound continuum states. The sources of $\overline{B}_{ba12}^{v'c'vc}$ are induced by the many-body Coulomb interaction Vpp.

For type-I structures, the linear response originating from intrawell excitations is fully described by p^{11} and p^{22}. Additional contributions from the interwell exciton coherences p^{31} and p^{42} have to be considered for type-II structures. Two-exciton coherences $\overline{B}$ are generated in second order by interacting once with the pump and once with the probe field. For co-circular excitation conditions ($\sigma^+\sigma^+$), only unbound continuum states are excited, whereas bound biexcitons contribute for counter-circularly polarized fields ($\sigma^+\sigma^-$). The total nonlinear response in third order within the coherent $\chi^{(3)}$ limit is given by p^{11} (X), p^{22} (X), p^{31} (CTX), and p^{42} (CTX).

The nonlinear optical response depends strongly on the polarization directions of the pump and probe fields. We therefore account for the vector nature of the dipole matrix element $\boldsymbol{\mu}$, the electric field $\mathbf{E}$, and the resulting optical polarization $\mathbf{P}$. The latter is obtained by summing up over all microscopic single-exciton polarizations $\mathbf{P}$ [34,35]:

$$\mathbf{P} = \sum_{ijvc}\boldsymbol{\mu}_{ij}^{vc}p_{ij}^{vc}. \qquad (5)$$

The experiment is performed with two pulses that propagate in the directions $\mathbf{k}_1$ and $\mathbf{k}_2$. Hence, we describe the incident electric field within the rotating wave approximation (RWA) by [26,35]

$$\begin{aligned}
&\mathbf{E}(t) = \mathbf{e}_1E_1(t)e^{i(\mathbf{k}_1\cdot\mathbf{r}-\omega_1t)} + \mathbf{e}_2E_2(t)e^{i(\mathbf{k}_2\cdot\mathbf{r}-\omega_2t)}, \\
&\text{with } E_1(t) \propto e^{-\left(\frac{t+\tau}{\Delta t_1}\right)^2} \text{ and } E_2(t) \propto e^{-\left(\frac{t}{\Delta t_2}\right)^2}. \qquad (6)
\end{aligned}$$

The polarization vectors of the electric fields are denoted $\mathbf{e}_1$ and $\mathbf{e}_2$, ω_1 and ω_2 (Δt_1 and Δt_2) represent their central frequencies (duration), respectively, and τ denotes the time delay between the two pulses. Following Refs. [26,34,35] we obtain the differential absorption which is measured in a pump-probe

experiment via

$$\Delta\alpha(\omega,\tau)\propto \mathrm{Im}\left[\int (\mathbf{e}_2)^*\cdot\delta\mathbf{P}(t,\tau)e^{i\omega t}dt\right]. \tag{7}$$

The numerical parameters in this simulation are quite similar to those used in several previous studies, see, e.g., Ref. [35] and references therein. These values are chosen in order to match known properties of the investigated quantum-well systems, e.g., the exciton and biexciton binding energies, as well as the dephasing times, and the strength of exciton resonances in the linear absorption. Here we use tight-binding couplings $T_{ij}^{v/c}=J_{v/c}$ with $|i-j|=1$ of $J_c=14$ meV and $J_v=0.7$ meV describing the couplings between neighboring sites in the conduction bands and the heavy-hole (hh) bands, respectively.

The dipole matrix elements are denoted μ_{ij}^{vc} and the nonvanishing transitions are given by

$$\mu_{ij}^{11}=\delta_{ij}\frac{\mu_{\text{type I}}}{\sqrt{2}}\begin{pmatrix}1\\ i\end{pmatrix},\quad \mu_{ij}^{22}=\delta_{ij}\frac{\mu_{\text{type I}}}{\sqrt{2}}\begin{pmatrix}1\\ -i\end{pmatrix},$$

$$\mu_{ij}^{31}=\delta_{ij}\frac{\mu_{\text{type II}}}{\sqrt{2}}\begin{pmatrix}1\\ i\end{pmatrix},\quad \mu_{ij}^{42}=\delta_{ij}\frac{\mu_{\text{type II}}}{\sqrt{2}}\begin{pmatrix}1\\ -i\end{pmatrix}. \tag{8}$$

Thus there is no optical coupling between the spin subspaces, i.e., $\mu_{ij}^{12}=\mu_{ij}^{21}=0$ and $\mu_{ij}^{32}=\mu_{ij}^{41}=0$. For the relative strength of the direct and indirect dipole matrix elements we use $\mu_{\text{type II}}=0.4\mu_{\text{type I}}$ which provides good agreement with the measured ratio of the optical absorption of the direct and the indirect exciton. Additionally, we use phenomenological dephasing times $\frac{1}{\gamma_p}$ and $\gamma_{\bar{B}}=2\gamma_p$. The dephasing times of the X and CTX are taken as $T_p=0.8$ ps and $T_p=4$ ps, respectively, which again matches experimental results [17].

The Coulomb matrix elements are given by

$$V_{ij}^{vv'}=U_0\frac{1}{|i-j|+a^{vv'}}, \tag{9}$$

with the regularization parameter $a^{vv'}$. For the Coulomb interactions within a quantum well, the regularization parameter is chosen, as in several previous studies, see, e.g., [35] and references therein, as $a^X=0.5$. Together with taking the strength of the interaction as $U_0=8.3$ meV this leads to a binding energy of the direct exciton X of about 7 meV and also a binding energy of the direct biexciton which matches experimental results [15]. To describe the reduced attraction between electrons and holes in different quantum wells the regularization parameters a^{31} and a^{42} are increased to $a^{CTX}=0.72$ which leads to a CTX binding energy of about 4.7 meV, in agreement with experiment.

Within our model, for type-I QW systems the differential absorption for counter-circularly polarized pump and probe pulses ($\sigma^+\sigma^-$) is entirely given by the correlation contribution CI_{corr} [26,27,35].

For $\sigma^+\sigma^-$ excitation the Pauli blocking (PB) contribution vanishes since the optical transitions do not couple the two spin subspaces. The CI_{1st} Hartree-Fock contribution $\propto p_{ba}^{v'c'*}p_{ba}^{v'c'}p_{12}^{vc}$ has a structure that in general may lead to a coupling between the spin subspaces:

$$\partial_t p_{12}^{vc}\propto\sum_{abv'c'}\left(V_{a2}^{c'c}-V_{a1}^{c'v}-V_{b2}^{v'c}+V_{b1}^{v'v}\right)\left(p_{ba}^{v'c'}\right)^*p_{ba}^{v'c'}p_{12}^{vc}. \tag{10}$$

However, for homogeneous systems the right-hand side of Eq. (10) vanishes. This can be easily understood by the fact that, in a homogeneous system, the relation $p_{ba}^{vc}=p_{ab}^{vc}$ is fulfilled since the electron-hole coherence depends only on the relative distance. Thus, the product between the coherences on the right-hand side of Eq. (10) is a symmetric function $g(a,b)=g(b,a)=(p_{ba}^{v'c'})^*p_{ba}^{v'c'}p_{12}^{vc}=(p_{ab}^{v'c'})^*p_{ab}^{v'c'}p_{12}^{vc}$ with respect to interchanging the site indices a and b. However, the prefactor $f(a,b)=(V_{a2}^{c'c}-V_{a1}^{c'v}-V_{b2}^{v'c}+V_{b1}^{v'v})$ changes its sign when a and b are interchanged. Consequently, the sum over the sites a and b appearing in Eq. (10) vanishes and a CI_{1st} contribution does not exist in a homogeneous system [26,27,29,35].

The situation changes when spatially indirect transitions are included by the valence bands $v=3,4$, see Fig. 2. In this case $p_{ba}^{vc}=p_{ab}^{vc}$ is still fulfilled and a and b denote spatial sites in a direction within the plane of the quantum wells. However, $f(a,b)=(V_{a2}^{c'c}-V_{a1}^{c'v}-V_{b2}^{v'c}+V_{b1}^{v'v})$ is no longer asymmetric with respect to interchanging a and b because we have to take into account the different Coulomb interactions within one well and between the two wells, i.e., the different regularization parameters a^X and a^{CTX}. This leads to a finite coupling of the spin subspaces already on the time-dependent Hartree-Fock level which, as is shown below, significantly modifies the nonlinear optical response of the CTX. As a result, in particular, the polarization direction dependence of the absorption changes at the CTX differ qualitatively from that at the direct exciton.

IV. RESULTS AND DISCUSSION

Experimental differential absorption signals ($\Delta\alpha L$) obtained at optimal temporal overlap for circularly polarized pump and probe pulses are presented in Fig. 3. The left-hand panel depicts the data for the co-circular polarization geometry while the right-hand panel presents the corresponding data for the counter-circular polarization-geometry data. Significant differential absorption signatures are only observed when the pump and the probe overlap in time. Both polarization configurations exhibit similar spectral characteristics in the differential absorption of the CTX resonance. This includes a discernible bleaching signature accompanied by a substantial blueshift, which remains consistent regardless of the polarization configuration of the pump and probe pulses. However, the differential signal is more pronounced for co-circular polarization compared with the counter-circular polarization configuration.

These coherent nonlinear optical responses of the CTX distinctly contrast the AC Stark effect observed in spatially direct QWs [27,40,41]. Notably, the nonlinearities for the spatially direct exciton resonances in the type-II heterostructure show a behavior consistent with the well-established AC Stark effect in spatially direct structures where lower energy states for electrons or holes are not present in adjacent layers. Co-circularly polarized pulses induce a blueshift in the

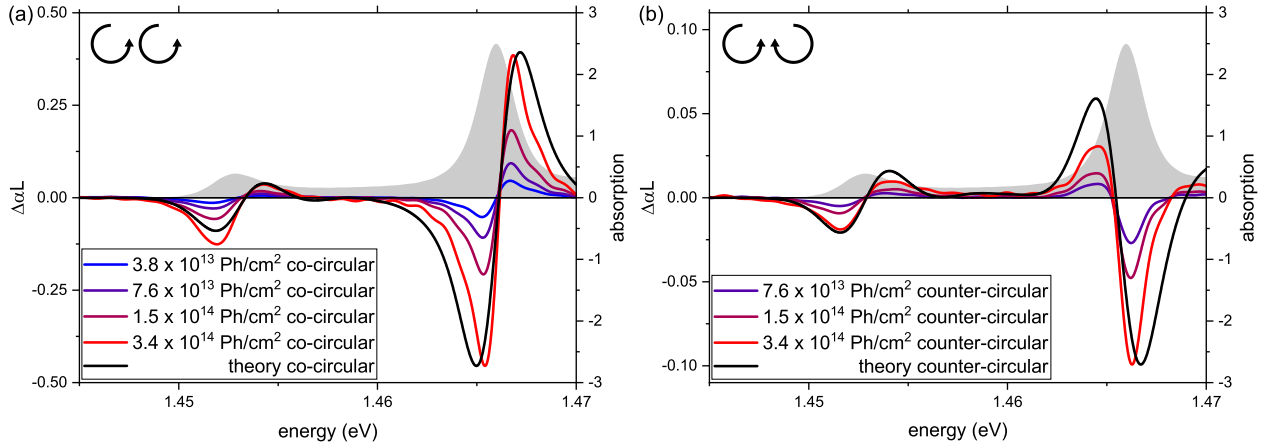

FIG. 3. Differential absorption signals ($\Delta\alpha L$) obtained experimentally for various pump pulse densities. Panel (a) shows data for the co-circular polarization geometry, while panel (b) shows data for the counter-circular polarization geometry. For reference, the linear absorption spectrum of the sample is given as a gray-shaded area. Both polarization configurations show a blueshift and a bleaching of the CTX absorption line while the spatially direct exciton in the (Ga, In)As layer (1.467 eV) exhibits the established responses, i.e., a blueshift for co-circular polarization and a redshift for counter-circular polarization of the pump and probe pulses. The solid black lines in both graphs represent the theoretical curves, normalized with respect to the minimum of the direct exciton absorption signal for the maximum pump density.

spatially direct resonance, while counter-circularly polarized pulses result in a redshift. This observation effectively negates any suggestions that the blueshift observed for the CTX could be attributed to disorder-induced effects.

Comparing the differential absorption spectra of the two types of QW excitons, namely, CTX and spatially direct excitons, in a PP configuration reveals key differences in their nonlinear response when pumping below the CTX resonance. These differences are a direct consequence of the distinct spatial configurations of the electrons and holes in the two types of structures. Comparing the experimental pump-induced absorption changes to the results from the calculations in Fig. 3 clearly shows that the theory correctly describes the AC Stark effect at both, the CTX and the type-I exciton resonance of the (Ga, In)As QW at 1.467 eV [27]. Specifically, both theory and experiment reveal a slightly asymmetric blueshift accompanied by a decrease in absorption at the CTX resonance for both polarization configurations. The nonlinear response at the CTX resonance exhibits similarities to the blueshift observed at the direct excitons in the (Ga, In)As layer when employing co-circularly polarized pulses. However, the additional bleaching of the absorption is specific to the CTX resonance and is not observed at the regular exciton resonance. This high level of agreement indicates that the outlined theoretical framework effectively captures all necessary features. The few remaining differences between the experimental and calculated spectra, particularly in the amount of bleaching at the CTX resonance for co-circularly polarized pulses, suggest the presence of additional factors influencing the nonlinear response at the CTX resonance that are not accounted for in the current theoretical analysis. A clear distinction in the response of the CTX compared with the type-I excitons becomes apparent for counter-circular polarization conditions. In this scenario, the CTX resonance exhibits a blueshift, contrasting with type-I QW heterostructures where the presence of bound biexcitons leads to a redshift. The origin of this blueshift becomes evident through the theoretical switch-off analysis shown in Fig. 4. Here, only the first-order Coulomb interaction leads to a blueshift of the CTX resonance for a counter-circular polarization geometry. This first-order

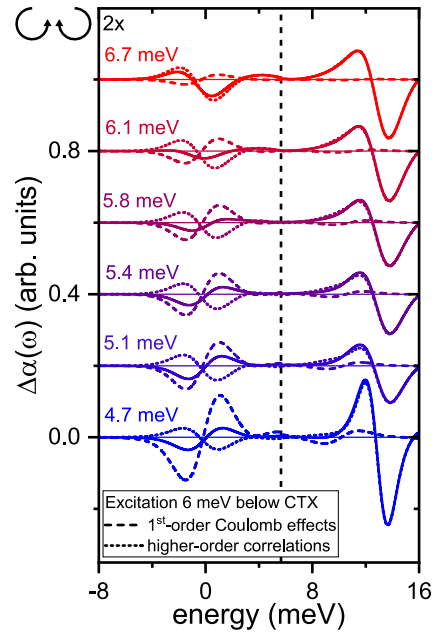

FIG. 4. Variation of the CTX binding energy with a fixed excitation detuning of 6 meV below the CTX resonance for counter-circular pump-probe polarizations. The dashed line corresponds to the first-order Coulomb contributions, while the dotted line represents higher-order Coulomb correlations. At low CTX binding energies, the first-order contributions dominate, inducing a net blueshift. Conversely, for high CTX binding energies, the higher-order correlations become prominent, leading to a redshift of the CTX. Please note that the zero of the energy scale corresponds to the CTX resonance and the CTX components are multiplied by a factor of two for better visibility.

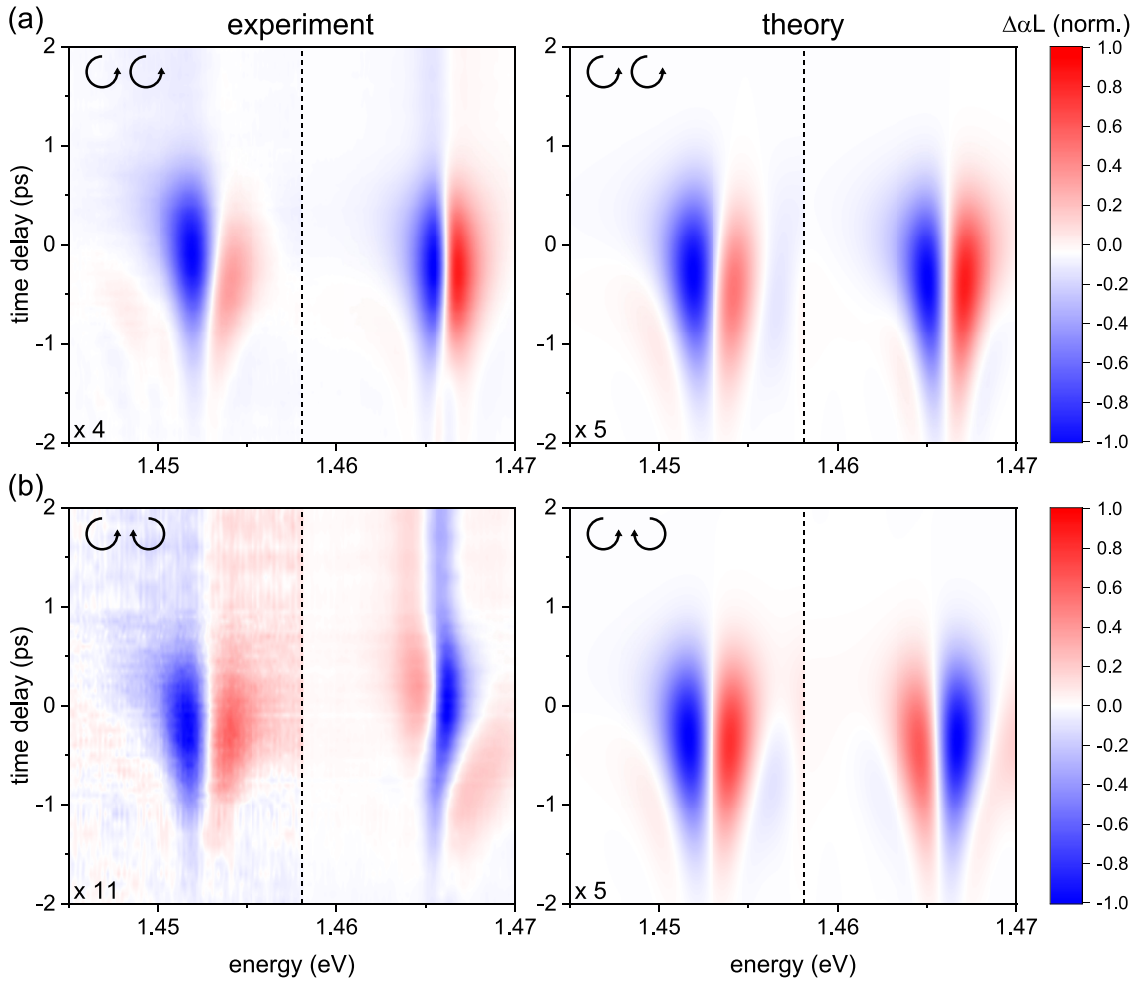

FIG. 5. 2D representation of the dynamics of the $\Delta\alpha L$ signals in both experiment and theory. The top row shows the co-circular polarization configurations for experiment (left) and theory (right). The bottom row shows the corresponding counter-circular polarization configurations. To enhance visibility, both the minimum value of the differential absorption in all contour plots is normalized to -1 at the energy associated with the type-I exciton transition in the (Ga, In)As layer and the lower-energy parts of the spectra containing the CTX (left side of the dotted line) are magnified by the factors are given in the respective bottom-left corners.

Coulomb interaction is uniquely present in inhomogeneous systems and dominates the redshifting higher-order correlations for CTX binding energies below 6 meV.

Closely analyzing the CI_{1st} term reveals that the hole and electron involved correspond to spatially separated layers, with $v = 4$ and $c = 2$, respectively.

Performing calculations for different binding energies of the CTX (which is achieved by varying the regularization parameter a^{CTX} which is described in Sec. III) for a fixed-detuning of 6 meV below the CTX resonance yields observable changes in the absorption response (refer to Fig. 4). A comparatively small binding energy of 4.7 meV, which describes the experimental data well, leads to a blueshift. Increasing the CTX binding energy in the theoretical calculations to around 6 meV leads to the appearance of a bleaching effect only. Here, the first-order contributions and the higher-order correlations are approximately equal and compensate each other. Any further increases of the binding energy weaken the first-order effect while the higher-order effects persist which then results in a redshift of the signal rather than the originally observed blueshift. Notably, at the direct X resonance, only the signal amplitude changes for the different CTX binding energies, while the spectral shift consistently remains a redshift.

The theoretical framework extends beyond spectral properties to include dynamic predictions within the coherent $\chi^{(3)}$ limit, which is applicable to negative time delays and near zero time. This dynamic facet of the analysis is visualized in Fig. 5, where we compare the temporal dynamics of the observed AC Stark shifts between experimental data and theory. Remarkably, our theoretical model not only impeccably reproduces the spectral properties when there is perfect temporal overlap of pump and probe pulses but also provides an accurate description of the temporal evolution of the AC Stark shifts. In particular, we find excellent agreement between the experimental and theoretical dynamics of the AC Stark shift for both the CTXs and type-I excitons, for both the co-circularly polarized pulses and the counter-circularly polarized pulses. However, for the latter case, the type-I transition exhibits a slightly delayed appearance of the redshift in the experimental results compared with the blueshift observed in the CTX resonance which is not reflected in our theoretical predictions.

Additionally, a minor deviation between theory and experiment surfaces at later delay times. Here, the experiment reveals weak spectral features due to residual incoherent excitons in the sample not considered in the theoretical framework. Overall, the remarkable agreement between theory and experiment underlines the comprehensive capability of our applied theoretical framework. It successfully predicts not only the spectral properties but also the intricate temporal dynamics, thereby providing valuable insights into the underlying nonlinear physics governing type-II systems.

V. CONCLUSION

We present a comprehensive experimental and theoretical analysis aimed at revealing the microscopic mechanism behind the optical Stark effect in charge-transfer excitons in high-quality (Ga, In)As/Ga(As, Sb) type-II heterostructures. The experimental pump probe spectra are well described by a microscopic model based on the SBE taking into account the permanent dipole moment inherent to the CTXs. A switch-off analysis reveals its importance for the observed differential absorption features and how it results in a blueshift of the CTX resonance for both, co-circular and counter circular polarization configurations, contrary to shifts of spatially direct exciton resonances.

ACKNOWLEDGMENTS

Financial support from the Deutsche Forschungsgemeinschaft via the Collaborative Research Center SFB 1083 (Project No. 223848855) and the Transregional Collaborative Research Center TRR 142 "Tailored Nonlinear Photonics" (Project No. 231447078, Subproject No. A10) is gratefully acknowledged. We thank the Paderborn Center for Parallel Computing (PC^2) for a computing time grant.

[1] J. Shah, *Ultrafast Spectroscopy of Semiconductors and Semiconductor Nanostructures*, Springer Series in Solid-State Sciences (Springer, Berlin, Heidelberg, 2013).
[2] J. Singh, in *Optical Properties of Condensed Matter and Applications*, edited by J. Singh (John Wiley & Sons, 2006), Vol. 6.
[3] S. Schmitt-Rink, D. Chemla, and D. A. Miller, Adv. Phys. **38**, 89 (1989).
[4] A. Von Lehmen, D. S. Chemla, J. Zucker, and J. P. Heritage, Opt. Lett. **11**, 609 (1986).
[5] Y.-H. Kuo, Y. K. Lee, Y. Ge, S. Ren, J. E. Roth, T. I. Kamins, D. A. Miller, and J. S. Harris, Nature (London) **437**, 1334 (2005).
[6] D. A. B. Miller, D. S. Chemla, T. C. Damen, A. C. Gossard, W. Wiegmann, T. H. Wood, and C. A. Burrus, Phys. Rev. Lett. **53**, 2173 (1984).
[7] M. Stepanenko, I. Kulinich, and I. Yunusov, J. Phys.: Conf. Ser. **1145**, 012028 (2019).
[8] H. Yamamoto, M. Asada, and Y. Suematsu, J. Lightwave Technol. **6**, 1831 (1988).
[9] T. Aizawa, K. Ravikumar, S. Suzaki, T. Watanabe, and R. Yamauchi, IEEE J. Quantum Electron. **30**, 585 (1994).
[10] A. Barenco, D. Deutsch, A. Ekert, and R. Jozsa, Phys. Rev. Lett. **74**, 4083 (1995).
[11] T. Unold, K. Mueller, C. Lienau, T. Elsaesser, and A. D. Wieck, Phys. Rev. Lett. **92**, 157401 (2004).
[12] C. Chakraborty, K. M. Goodfellow, S. Dhara, A. Yoshimura, V. Meunier, and A. N. Vamivakas, Nano Lett. **17**, 2253 (2017).
[13] A. Muller, W. Fang, J. Lawall, and G. S. Solomon, Phys. Rev. Lett. **103**, 217402 (2009).
[14] A. Laucht, J. M. Villas-Bôas, S. Stobbe, N. Hauke, F. Hofbauer, G. Böhm, P. Lodahl, M.-C. Amann, M. Kaniber, and J. J. Finley, Phys. Rev. B **82**, 075305 (2010).
[15] M. Stein, C. Lammers, P.-H. Richter, C. Fuchs, W. Stolz, M. Koch, O. Vänskä, M. J. Weseloh, M. Kira, and S. W. Koch, Phys. Rev. B **97**, 125306 (2018).
[16] C. Meineke, M. Prager, J. Hayes, Q. Wen, L. Z. Kastner, D. Schuh, K. Fritsch, O. Pronin, M. Stein, F. Schäfer, S. Chatterjee, M. Kira, R. Huber, and D. Bougeard, Light: Sci. Appl. **11**, 151 (2022).
[17] M. Fey, M. Stein, C. Fuchs, W. Stolz, K. Volz, and S. Chatterjee, Phys. Rev. B **106**, 165303 (2022).
[18] F. Schäfer, M. Stein, J. Lorenz, F. Dobener, C. Ngo, J. T. Steiner, C. Fuchs, W. Stolz, K. Volz, T. Meier, J. Hader, J. V. Moloney, S. W. Koch, and S. Chatterjee, Appl. Phys. Lett. **122**, 082104 (2023).
[19] C. Berger, C. Möller, P. Hens, C. Fuchs, W. Stolz, S. W. Koch, A. Ruiz Perez, J. Hader, and J. V. Moloney, AIP Adv. **5**, 047105 (2015).
[20] C. Möller, C. Fuchs, C. Berger, A. Ruiz Perez, M. Koch, J. Hader, J. V. Moloney, S. W. Koch, and W. Stolz, Appl. Phys. Lett. **108**, 071102 (2016).
[21] C. Lammers, M. Stein, C. Berger, C. Möller, C. Fuchs, A. Ruiz Perez, A. Rahimi-Iman, J. Hader, J. V. Moloney, W. Stolz, S. W. Koch, and M. Koch, Appl. Phys. Lett. **109**, 232107 (2016).
[22] G. G. Zegrya and A. D. Andreev, Appl. Phys. Lett. **67**, 2681 (1995).
[23] J. I. Malin, J. R. Meyer, C. L. Felix, J. R. Lindle, L. Goldberg, C. A. Hoffman, F. J. Bartoli, C.-H. Lin, P. C. Chang, S. J. Murry, R. Q. Yang, and S.-S. Pei, Appl. Phys. Lett. **68**, 2976 (1996).
[24] J. R. Meyer, C. L. Felix, W. W. Bewley, I. Vurgaftman, E. H. Aifer, L. J. Olafsen, J. R. Lindle, C. A. Hoffman, M.-J. Yang, B. R. Bennett, B. V. Shanabrook, H. Lee, C.-H. Lin, S. S. Pei, and R. H. Miles, Appl. Phys. Lett. **73**, 2857 (1998).
[25] W. H. Knox, D. S. Chemla, D. A. B. Miller, J. B. Stark, and S. Schmitt-Rink, Phys. Rev. Lett. **62**, 1189 (1989).
[26] C. Sieh, T. Meier, A. Knorr, F. Jahnke, P. Thomas, and S. W. Koch, Eur. Phys. J. B **11**, 407 (1999).
[27] C. Sieh, T. Meier, F. Jahnke, A. Knorr, S. W. Koch, P. Brick, M. Hübner, C. Ell, J. Prineas, G. Khitrova, and H. M. Gibbs, Phys. Rev. Lett. **82**, 3112 (1999).
[28] S. W. Koch, C. Sieh, T. Meier, F. Jahnke, A. Knorr, P. Brick, M. Hübner, C. Ell, J. Prineas, G. Khitrova, and H. Gibbs, J. Lumin. **83-84**, 1 (1999).

[29] A. Trautmann, M. Stein, F. Schäfer, D. Anders, C. Ngo, J. T. Steiner, M. Reichelt, S. Chatterjee, and T. Meier, Proc. SPIE **12419**, 124190A (2023).
[30] M. Lindberg, Y. Z. Hu, R. Binder, and S. W. Koch, Phys. Rev. B **50**, 18060 (1994).
[31] V. M. Axt and A. Stahl, Z. Phys. B: Condens. Matter **93**, 195 (1994).
[32] V. M. Axt and A. Stahl, Z. Phys. B: Condens. Matter **93**, 205 (1994).
[33] W. Schäfer, D. S. Kim, J. Shah, T. C. Damen, J. E. Cunningham, K. W. Goossen, L. N. Pfeiffer, and K. Köhler, Phys. Rev. B **53**, 16429 (1996).
[34] H. Haug and S. W. Koch, *Quantum Theory of the Optical and Electronic Properties of Semiconductors*, 5th ed. (World Scientific, Singapore, 2009).
[35] T. Meier, P. Thomas, and S. W. Koch, *Coherent Semiconductor Optics: From Basic Concepts to Nanostructure Applications* (Springer, New York, 2007).
[36] S. Weiser, T. Meier, J. Möbius, A. Euteneuer, E. J. Mayer, W. Stolz, M. Hofmann, W. W. Rühle, P. Thomas, and S. W. Koch, Phys. Rev. B **61**, 13088 (2000).
[37] S. Chatterjee, C. Ell, S. Mosor, G. Khitrova, H. M. Gibbs, W. Hoyer, M. Kira, S. W. Koch, J. P. Prineas, and H. Stolz, Phys. Rev. Lett. **92**, 067402 (2004).
[38] W. Hoyer, C. Ell, M. Kira, S. W. Koch, S. Chatterjee, S. Mosor, G. Khitrova, H. M. Gibbs, and H. Stolz, Phys. Rev. B **72**, 075324 (2005).
[39] J. E. Sipe and E. Ghahramani, Phys. Rev. B **48**, 11705 (1993).
[40] P. Brick, C. Ell, S. Chatterjee, G. Khitrova, H. M. Gibbs, T. Meier, C. Sieh, and S. W. Koch, Phys. Rev. B **64**, 075323 (2001).
[41] N. S. Köster, K. Kolata, R. Woscholski, C. Lange, G. Isella, D. Chrastina, H. von Känel, and S. Chatterjee, Appl. Phys. Lett. **98**, 161103 (2011).